Modulation of the magnetoimpedance effect of ZnO:Ag/NiFe heterostructures by thermal annealing

A. Ferreira and F. Vaz
Centro de Física, Universidade do Minho, 4710-057 Braga, Portugal

M. A. Correa and F. Bohn
Departamento de Física Teórica e Experimental,
Universidade Federal do Rio Grande do Norte, 59078-900 Natal, RN, Brazil

S. Lanceros-Méndez
IKERBASQUE, Basque Foundation for Science, E-48013 Bilbao, Spain and
BCMaterials, Basque Center for Materials, Applications and Nanostructures, UPV/EHU Science Park, 48940 Leioa, Spain.
(Dated: November 18, 2019)

The magnetization dynamics in ZnO:Ag/NiFe heterostructures has been investigated through magnetoimpedance measurements. By annealing the ZnO:Ag layer during the production process of the samples, structural and magnetic features of the whole heterostructure are modified, showing that the dynamical magnetic response of the heterostructure is strongly dependent on the annealing temperature. The magnetoimpedance results are discussed in terms of the different mechanisms governing the magnetization dynamics at distinct frequency ranges and in terms of the evolution of the ZnO:Ag layer with annealing. The presented results open new roads for technological application of semiconductor/ferromagnetic heterostructures.

Keywords: ZnO, Permalloy, Magnetization dynamics, Magnetoimpedance effect

I. INTRODUCTION

Magnetoimpedance (MI) has provided in the last decades new roads to technological applications[1–4]. Further, it also represents an important tool to understand the basic physical properties of the magnetization dynamics in films and heterostructures[5,6]. Specifically, MI corresponds to the change of the complex electrical impedance ($Z = R + iX$) of a magnetic material submitted to an external magnetic field[7,8]. For an ordinary metallic ferromagnetic material in the film or ribbon geometries, the MI variations at frequencies up to hundreds of MHz are primarily associated to changes in the transverse magnetic permeability (μ_t) due to modifications in the skin effect[7,8]. At frequencies above GHz, in turn, the ferromagnetic resonance (FMR) effect emerges, becoming the main contribution to the variations in the electrical impedance and, consequently, to the MI variations.

The MI effect has been explored in a wide variety of samples[9–11], giving rise to a broad range of remarkable results. Among the different geometries, planar heterostructures consisting of a bilayer with a magnetic material and a non-magnetic metal/semiconductor have been drawing considerable attention due to the perspective of application in spintronics[12,13]. One of the most paradigmatic materials in this field is $Y_3Fe_5O_{12}$ (YIG), a ferrimagnetic insulator that, when capped by a non-magnetic metal with high spin-orbit coupling, enables the evaluation of pure spin- current effects in films with bilayer geometry[5,6].

Another type of materials receiving increasing interest due to their magnetic properties corresponds to non-magnetic metal-doped semiconductors[14–16]. In this case, Zinc oxide (ZnO) arises as a notable representative. Beyond the well-known semiconductor and optical properties, ZnO can show ferromagnetism at room temperature (RTFM)[17], a fact directly related to the role of gain boundaries and the overlap of bound magnetic polarons (BMPs)[14,16].

Remarkably, this feature looks promising for spintronic applications, in particular due to the electrical properties of the material[18,19]. However, up to now, just a few works have explored the magnetization dynamics in semiconductor materials[20–22]. As an interesting example, Dadsetan et al[23] have recently investigated the magnetization dynamics in semiconductors exploring the MI effect in Fe-rich ribbons sandwiched by ZnO films. Specifically, the authors have analyzed the MI response in frequencies up to 10 MHz and evaluated the influence of ZnO layer thickness on the magnetic response[23], thus opening doors to investigations in such kind of heterostructures

In this context, the interplay between soft ferromagnetic films and semiconductor materials may bring to light heterostructures with potential technological applications through their integration in engineered devices. In this work, a systematic investigation of the magnetization dynamics has been performed in ZnO:Ag/NiFe heterostructures by magnetoimpedance. By annealing the ZnO:Ag layer during the production process of the samples, different structural and magnetic features of the whole heterostructure are modified. It is observed that the dynamical magnetic response of the heterostructure is strongly dependent on the annealing temperature.

II. MATERIALS AND METHODS

Heterostructures consisting of a 1 μm-thick ZnO:Ag film capped by a NiFe layer with thickness of 200 nm have been investigated. The production of the samples was performed in two steps. First, the ZnO:Ag films were deposited on a glass substrate using DC sputtering from a metallic Zinc target (99.96 at.% purity and dimensions of 20 x 10 x 0.6 cm^3). In particular, the Zn target was decorated with specific amount of Ag pellets, symmetrically distributed along the main erosion area (50 cm^2)[24], in order to set the silver concentration at 20 wt.% in the produced layer. This deposition was carried out with the following parameters: base pressure of 6 10^{-7} Torr, deposition pressure of 5 10^{-3} Torr with Ar at 25 sccm and O_2 at 16 sccm constant flows, and 377 V set in the DC source. After ZnO:Ag deposition, the substrate was cut in 3 pieces, and two of them were annealed. Thus, a set of films is obtained composed by the as-cast sample and the films annealed at distinct conditions, 250 and 400°C. In the second step, $Ni_{81}Fe_{19}$ (NiFe) is grown to cover the ZnO:Ag films. In particular, the NiFe layer is deposited considering a base pressure of 2 10^{-8} Torr, deposition pressure of 3 10^{-3} Torr with Ar at 20 sccm constant flow, and 20 W set in the RF source.

The structural properties of the films were investigated by X-ray diffraction (XRD) and the morphological ones by scanning electron microscopy (SEM). XRD results were acquired using a Rigaku Miniflex II diffractometer in the Bragg-Brentano geometry. In this case, the XRD analysis was performed for the as-cast and annealed bare ZnO:Ag films, as well as for the samples after the deposition of the NiFe cap layer. SEM images of the ZnO:Ag/NiFe heterostructures were obtained with a NanoSEM - FEI Nova 200 (FEG/SEM) microscope, on fractured cross-sections and top views conditions.

The quasi-static magnetic characterization of the bare ZnO:Ag films and ZnO:Ag/NiFe heterostructures was performed using a Lake Shore model 7404 vibrating sample magnetometer (VSM). In this case, the in-plane magnetic behavior was obtained from the magnetization curves measured at room temperature.

The magnetization dynamics of the ZnO:Ag/NiFe heterostructures was investigated through the MI effect. To this end, a RF-impedance analyzer Agilent model E4991 was used, provided with a E4991A test head connected to a microstrip, in which the sample is the central conductor that is separated from the ground plane by the substrate, as depicted in Fig. 1. To avoid propagative effects and to acquire just the sample contribution to MI, the RF impedance analyzer was calibrated at the end of the connection cable by performing open, short, and load (50 Ω) measurements using reference standards. While the external magnetic field was varied, a 0 dBm (1 mW) constant power was applied to the sample, characterizing a linear regime of driving signal. MI measurements were obtained over a frequency range between 0.5 and 3.0 GHz, with in-plane magnetic field varying between 350 Oe. For each magnetic field value, the frequency sweep was carried out and the real R and imaginary X components of the impedance Z were simultaneously acquired.

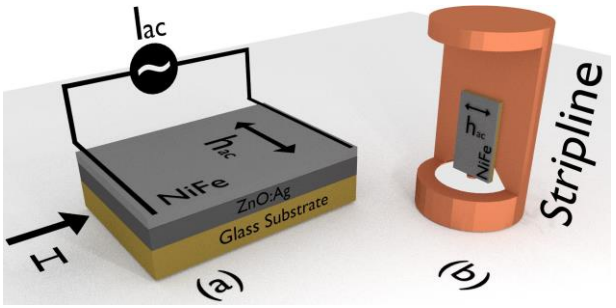

FIG. 1. Schematic representation of the ZnO:Ag/NiFe heterostructure in the MI experiment. (a) In detail, in-plane magnetic field H and alternating magnetic field h_{ac} acting simultaneously in the sample. (b) Stripline used for the MI measurement.

III. RESULTS AND DISCUSSION

Figure 2 presents the results of the structural characterization of the ZnO:Ag/NiFe heterostructures.

From the XRD data shown in Fig. 2(a), the patterns clearly indicate the hexagonal structure for the ZnO phase (space group p6122), assigned by the (100), (101), and (110) peaks located respectively at $2\theta = XX^\circ$, XX°, and XX° (ICSD card #01-070-8070), feature which is found for all samples. Further, with the increase of the annealing temperature, it is observed the increase of the peaks matching those of pure Ag at 2θ = 38.12°, and 44.31°, corresponding to the (111) and (200) crystallographic planes of face-centered cubic Ag crystals (ICSD card #01-071-6549). This feature is attributed to the migration of the Ag clusters to the film surface as the annealing temperature increases, a fact confirmed by the SEM images. The peak related to the (111) $Ni_{81}Fe_{19}$ plane (ICSD card #01-088-1715) is located at 2θ = 44.07°, close to the one associated to the reflection of the (200) Ag, in a sense that they overlap.

Figs. 2(b,c) show representative SEM images for bare ZnO:Ag films annealed at 400°C and the corresponding heterostructure. In particular, from the top-view SEM image of the bare film, it is confirmed that the Ag layer fully covers the ZnO film. In addition, the cross-section SEM image for the ZnO:Ag/NiFe heterostructure reveals the columnar growth of both, the ZnO and NiFe layers, as well as corroborates the good interface between them.

Regarding the magnetic behavior, Fig. 3 shows the room temperature normalized magnetization curves

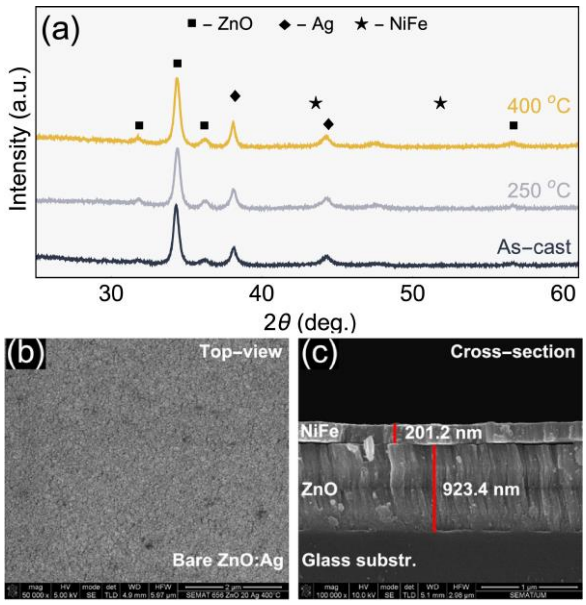

FIG. 2. Structural characterization of the ZnO:Ag/NiFe heterostructures. (a) XRD results for the ZnO:Ag/NiFe heterostructures produced from ZnO:Ag films annealed at different temperatures. The peaks are indexed by using the ICSD database and considering the patterns for ZnO (ICSD card #01-070-8070), Ag (#01-071-6549), and NiFe (#01-088-1715). (b) Representative top-view SEM image for the bare ZnO:Ag films annealed at 400°C. (c) Representative cross-section SEM image for the ZnO:Ag/NiFe heterostructures produced from the ZnO:Ag films annealed at 400°C.

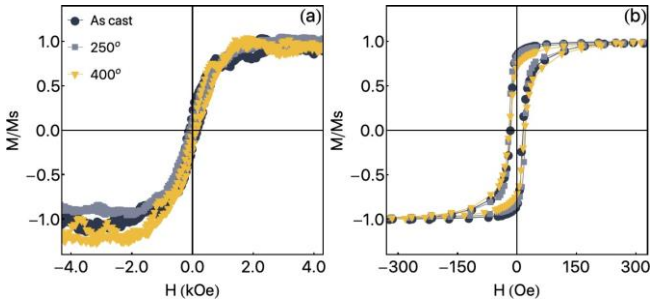

FIG. 3. Magnetic behavior of the produced samples. Magnetization curves acquired for (a) the bare ZnO:Ag films annealed at different temperatures and (b) the corresponding ZnO:Ag/NiFe heterostructures. The obtained magnetic parameters are summarized in Tab. I.

TABLE I. Coercive field H_c and normalized remnant magnetization M_r/M_s values obtained from the curves measured for the bare ZnO:Ag films annealed at different temperatures and the corresponding ZnO:Ag/NiFe heterostructures.

	ZnO:Ag		ZnO:Ag/NiFe	
Annealing	H_c (Oe)	M_r/M_s	H_c (Oe)	M_r/M_s
As-cast	145.42	0.25	17.06	0.84
250°C	111.21	0.17	20.83	0.83
400°C	65.45	0.09	19.39	0.70

obtained for the bare ZnO:Ag films annealed at different temperatures and the corresponding ZnO:Ag/NiFe heterostructures.

From the curves obtained for the ZnO:Ag films, Fig. 3(a), it can be identified the fingerprint of the room temperature ferromagnetism. This feature is expected for metal-doped ZnO films[15,16]. Specifically, the RTFM behavior in non-magnetic doped ZnO is associated with grain boundary effects and the overlap of bound magnetic polarons (BMPs)[14,16]. It is worth noting that the films saturate magnetically at magnetic fields of about 2 kOe. In particular, the curves were normalized in order to make easier the comparison between results. However, it is highlighted that the saturation magnetization of the bare ZnO:Ag films are found in the range between 0.5 and 1.6 emu/cm^3, values in agreement with previous results reported in the literature[21]. Table I summarizes the magnetic parameters obtained from the magnetization curves.

After the deposition of the NiFe layer, the magnetic behavior changes drastically, as expected. The magnetization responses for the ZnO:Ag/NiFe heterostructures, shown in Fig. 3(b), disclose characteristic curves of a soft ferromagnetic material, evidencing the magnetic properties of the NiFe layer. Here, the NiFe alloy determines the whole magnetic behavior of the heterostructures due to its high saturation magnetization, ~ 780 emu/cm^3 [25,26], much larger than that verified to ZnO:Ag. All heterostructures show the very same magnetic behavior, irrespective of the conditions employed in the ZnO:Ag annealing. It is characterized by low coercive field and high normalized remnant magnetization, as indicated in Tab. I Further, the shape and the area of the magnetization curves are evidence of the existence of some dispersion of the magnetic anisotropy, a feature expected due to the roughness of the interface between the NiFe and ZnO:Ag layers.

Finally, with respect to the magnetization dynamics characterization, Fig. 4 depicts the MI response for the ZnO:Ag/NiFe heterostructures. Here, to allow a direct comparison between the results, it is considered the normalized variation of the real R component of the impedance, defined as

$$\frac{\Delta R}{R} = \frac{R(H) - R(H_{max})}{R\,(H_{max})} \quad (1)$$

where $R(H)$ is the real component at a given external magnetic field H, and $R(H_{max})$ is the corresponding value at the maximum magnetic field value, where the samples are magnetically saturated.

Figure 4(a) shows the density plot of $\Delta R/R$ for the ZnO:Ag/NiFe heterostructures produced from the ZnO:Ag films annealed at 400°C, as a representative example of the MI behavior verified for the studied samples. By considering this two-dimensional plot, it is observe the $\Delta R/R$ behavior as a function of both external

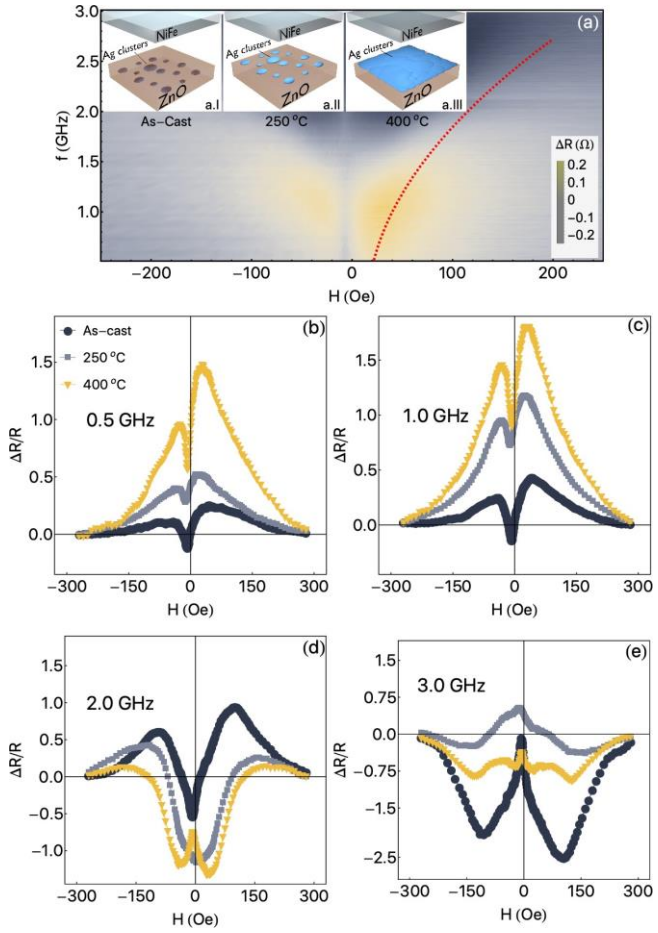

FIG. 4. Magnetoimpedance response for the ZnO:Ag/NiFe heterostructures. (a) Density plot of $\Delta R/R$ as a function of both, external magnetic field and frequency for the ZnO:Ag/NiFe heterostructures produced from the ZnO:Ag films annealed at 400°C. The red dashed line is a guide to the eyes, indicating the evolution of the $\Delta R/R$ peak location in field as the frequency increases. (b) $\Delta R/R$ measured at 0.5 GHz as a function of the external magnetic field for the ZnO:Ag/NiFe heterostructures. Similar plot for the $\Delta R/R$ response at (c) 1.0, (d) 2.0, and (e) 3.0 GHz.

magnetic field H and frequency f. Although the MI curves are acquired over a complete magnetization loop and present hysteretic behavior, just part of the curve is shown, with the field varying from negative to positive values. When the field varies from positive to negative values, the MI behavior is reversed. Despite the similar general MI response verified for the heterostructures produced from ZnO:Ag films annealed at different temperatures, a significant reduction of the amplitude of the impedance variation peaks is observed as the annealing temperature decreases. This feature is clearly confirmed by the plot of $\Delta R/R$ as a function of the magnetic field for selected frequencies, as shown in Fig. 4(b-e).

From Fig. 4(a), it is observed that the $\Delta R/R$ curves show a double peak structure. At the low and moderate frequency ranges (up to hundreds of MHz), the $\Delta R/R$ peaks are located at ± 20 Oe, close to the coercive field H_c verified from the magnetization curves (see Tab. I). Therefore, the peak position in field reflects the anisotropy field and, consequently, the magnetic anisotropy of the samples. Moreover, at this regime, the invariance of the position of the peaks is a clear indication that the skin effect is the main responsible for the MI variations. On the other hand, when also considering Fig. 4(c-d) for higher frequencies, besides the skin effect, the FMR effect also becomes an important mechanism responsible by the MI variations, a fact evidenced by the displacement of the peaks position toward higher field as the frequency is increased[27]. In particular, in Fig. 4(a), a red dashed line is drawn guiding the eyes in order to highlight the evolution of the peak location in field. For the frequency of 3.0 GHz, Fig. 4(e), the magnetic field is not enough to saturate the heterostructures and, as a consequence, characteristic negative $\Delta R/R$ peaks values are observed at low-magnetic fields[28].

Also in Fig. 4(b), where FMR does not influence the magnetization dynamics, it is remarkable the dependence of the amplitude of the $\Delta R/R$ peaks with the temperature employed in the annealing of the bare ZnO:Ag films. The trend of raising the peak amplitude is a result of the reduction of the roughness of the interface between the NiFe and ZnO:Ag layers, as well as it is associated with the changes in the electrical properties of the ZnO:Ag layer. More specifically, it is a consequence of the distribution of the Ag in the ZnO:Ag layer. For the ZnO:Ag/NiFe heterostrucutre produced from the as-cast ZnO:Ag film, the NiFe layer is primarily deposited onto a ZnO film (see the illustration a.I in Fig. 4(a)). However, with the increase of the annealing temperature, the top ZnO:Ag surface and the ZnO:Ag electrical properties change drastically. It is associated to the displacement of Ag clusters to the ZnO:Ag film surface (see a.II in Fig. 4(a)). When the annealing is performed at 400°C, a metallic layer of Ag emerge (see a.III in Fig. 4(a)). Hence, the conductor Ag layer reduces the whole electrical resistivity of the sample, leading to the increase of the MI variations.

Thus, from a general point of view, the explored heterostructures appears as a promising candidate for technological applications based on the soft ferromagnetic properties in the ZnO:Ag/NiFe heterostructures and the multifunctionalization of semiconductor materials with ferromagnetic alloys.

IV. CONCLUSION

In conclusion, the magnetization dynamics in ZnO:Ag/NiFe heterostructures has been investigated through the magnetoimpedance measurements. First, considering

the bare ZnO:Ag films, room temperature ferromagnetism is verified in non-magnetic metal-doped semiconductores. Further, by performing annealing of the ZnO:Ag films at different temperatures, the structural and magnetic features of the whole heterostructures have been modified. The heterostructures show soft ferromagnetic properties and the MI response is strongly dependent on the annealing temperature. More specifically, the MI response is affected directly by the distribution of the Ag in the ZnO:Ag layer, that changes the roughness of the interface between the NiFe and ZnO:Ag layers, as well as alters the electrical properties of the ZnO:Ag layer. The presented results open new ways for technological application of semiconductor/ferromagnetic heterostructures.

ACKNOWLEDGMENTS

This works was partially supported by the Brazilian agencies CNPq and CAPES. Further, this work was also supported by the Portuguese Foundation for Science and Technology (FCT) in the framework of the Strategic Funding UID/FIS/04650/2019 and project PTDC/BTM-MAT/28237/2017. A. Ferreira acknowledges the FCT for the Junior Research Contract. Financial support from the Basque Government under the ELKARTEK, HAZITEK and PIBA programs is also acknowledged.

* Electronic address: marciocorrea@dfte.ufrn.br

[1] Y. Wang, Y. Wen, P. Li, and L. Chen, Sensors Actuators A Phys. **284**, 112 (2018).
[2] G. V. Kurlyandskaya *et al.*, Appl. Phys. Lett. **82**, 3053 (2003).
[3] B. Li, M. N. Kavaldzhiev, and J. Kosel, J. Magn. Magn. Mater. **378**, 499 (2015).
[4] E. Fernández, G. V. Kurlyandskaya, A. García-Arribas, and A. V. Svalov, Nanoscale Res. Lett. **7**, 230 (2012).
[5] M. Correa *et al.*, J. Magn. Magn. Mater. **485**, 75 (2019).
[6] J. Santos, E. Silva, W. Rosa, F. Bohn, and M. Correa, Mater. Lett. **256**, 126662 (2019).
[7] R. S. Beach and A. E. Berkowitz, Appl. Phys. Lett. **64**, 3652 (1994).
[8] L. Kraus, Sensors Actuators, A Phys. **106**, 187 (2003).
[9] X. Li *et al.*, J. Alloys Compd. **730**, 17 (2018).
[10] L. Jamilpanah *et al.*, J. Phys. D. Appl. Phys. **50**, 155001 (2017).
[11] U. Kilic, C. A. Ross, and C. Garcia, Phys. Rev. Appl. **10**, 034043 (2018).
[12] D. Smolyakov *et al.*, Thin Solid Films **671**, 18 (2019).
[13] T. Dyer, A. Mohan, and P. Hopper, Semiconductor gmi magnetometer, 2014.
[14] J. M. D. Coey, M. Venkatesan, and C. B. Fitzgerald, Nat. Mater. **4**, 173 (2005).
[15] A. H. Shah, M. Basheer Ahamed, E. Manikandan, R. Chandramohan, and M. Iydroose, J. Mater. Sci. Mater. Electron. **24**, 2302 (2013).
[16] N. Ali *et al.*, Sci. Rep. **9**, 2461 (2019).
[17] A. Ferreira, N. Martin, S. Lanceros-Méndez, and F. Vaz, Thin Solid Films **654**, 93 (2018).
[18] S. J. Pearton *et al.*, J. Electron. Mater. **35**, 862 (2006).
[19] J. H. Kim, H. Kim, D. Kim, S. G. Yoon, and W. K. Choo, Solid State Commun. **131**, 677 (2004).
[20] Z. Ahmed Khan, A. Rai, S. Roy Barman, and S. Ghosh, Appl. Phys. Lett. **102**, 022105 (2013).
[21] M. He *et al.*, Appl. Phys. Lett. **99**, 222511 (2011).
[22] T. S. Herng *et al.*, Phys. Rev. Lett. **105**, 207201 (2010).
[23] A. Dadsetan, M. Almasi Kashi, and S. Mohseni, J. Magn. Magn. Mater. **493**, 165697 (2020).
[24] R. P. Domingues *et al.*, Vacuum **157**, 414 (2018).
[25] J. C. A. Huang, Y. M. Hu, C. C. Yu, C. H. Tsao, and C. H. Lee, Phys. Rev. B **57**, 11517 (1998).
[26] S. M. Zhou, K. Liu, and C. L. Chien, J. Appl. Phys. **87**, 6659 (2000).
[27] a. Yelon *et al.*, Appl. Phys. Lett. **69**, 3084 (1996).
[28] J. M. Barandiaran, A. Garcia-Arribas, and D. de Cos, J. Appl. Phys. **99**, 103904 (2006).